ELSEVIER

Polymer 41 (2000) 8615–8623

polymer

www.elsevier.nl/locate/polymer

The morphology of nascent and moulded ultra-high molecular weight polyethylene. Insights from solid-state NMR, nitric acid etching, GPC and DSC

J.T.E. Cook[a], P.G. Klein[a,*], I.M. Ward[a], A.A. Brain[b], D.F. Farrar[b], J. Rose[b]

[a]*IRC in Polymer Science and Technology, University of Leeds, Leeds LS2 9JT, UK*
[b]*Smith and Nephew Group Research Centre, York Science Park, Heslington, York YO10 5DF, UK*

Received 3 November 1999; received in revised form 14 March 2000; accepted 23 March 2000

Abstract

The differences in morphology between nascent ultra-high molecular weight polyethylene (UHMWPE) GUR415 grade powder and a ram-extruded moulded form have been studied by a variety of techniques. While it would be thought from DSC results that the powder has much thicker crystallites than the moulded material, it is shown quite clearly by nitric acid etching techniques followed by GPC that the crystal lamellae in both forms of the material have similar dimensions, close to 20 nm on average. The GPC also shows, however, that in addition to the lamellar material, there exists a proportion of extended chain crystals in the powder, which may reside within fibrillar structures which have been observed by SEM. NMR measurements show that the amorphous phase in the powder is more constrained than that of the moulded material, and that the powder also has a fraction of monoclinic crystalline material associated with internal stress. Further NMR experiments on the highly crystalline residues from the nitric acid degradation experiments lead to an estimation of the spin–lattice relaxation time in a 100% crystalline PE of 2.5 ± 0.1 s in an external field of 4.7 T.

Keywords: UHMWPE; Morphology; NMR

1. Introduction

Ultra High Molecular Weight Polyethylene (UHMWPE) has been the material of choice in total hip joint replacement operations since the late 1960s. It is used as the bearing surface of the acetabular cup in which a stainless steel femoral head articulates. There are many advantages for the use of this type of material in such orthopaedic applications, including its non-toxicity, high impact and abrasion resistances, and the low coefficient of friction when it is sliding on metals. A well-made implant can have a lifetime of up to 15 or more years, but there can be problems with severe wear, oxidation during sterilisation and fatigue fracture of the polyethylene component [1–7]. Despite the extended, extensive use of the material in the medical industry, it is only relatively recently that its morphology has been studied, to try to tailor the properties of the implants for optimising their success. Work has been done, looking at the effect of γ-sterilisation on the wear properties [8] but in the work presented here, we shall use unsterilised material to investigate the fundamental morphological aspects, avoiding complications induced on sterilisation, like chain scission, and changes in the density, introduction of oxidation products, etc.

There have been a number of studies of the general morphology of UHMWPE reported in the literature. Farrar and Brain [9] used a combination of optical microscopy, SEM, TEM and small-angle light scattering to study the unprocessed powder and the ram-extruded polymer. The powder appeared to comprise 50–250 μm particles, which are themselves agglomerates of of much finer 0.5–1.0 μm particles. Zachariades and Kanamoto [10] report that complete fusion of the reactor powder is only attained when processing temperatures of over 220°C are used. Below this, in the moulding the grain boundaries are still evident [9,10] and the incomplete fusion is associated with diminished mechanical properties. Morin et al. [11] used variable temperature high-resolution solid state NMR to study the morphologies of powder and moulded GUR413 UHMWPE, as well as the change in morphology when the temperature of the powder is increased. They also showed by differential scanning calorimetry (DSC) that the melting

* Corresponding author. Tel: + 44-113-2333814; fax: + 44-113-2333846.
E-mail address: p.g.klein@leeds.ac.uk (P.G. Klein).

0032-3861/00/$ - see front matter
PII: S0032-3861(00)00254-8

temperature of the crystals in the powder is much higher than that in the processed material. They associated this elevated melting temperature with a crystalline morphology possessing considerable strain, arising through crystallisation in a shear field created due to a temperature gradient at the polymerisation sites [12]. Tervoort-Engelen and Lemstra [13], who had seen a similar effect, asserted, however, that it may be due to a rapid annealing resulting in an increased apparent crystal thickness during melting. The high resolution NMR experiments [11] showed that the peak associated with the amorphous phase is not shifted as far from that of the orthorhombic phase in the powder as it is in the moulded material, due to a lower fraction of gauche conformations within the amorphous phase. As the temperature was raised, the position of the peak slowly moved upfield and the peak also became much narrower. They also saw that the resonance associated with the all-*trans* (crystalline) material was somewhat broader in the powder, reflecting the nature of the less perfect crystals. Valotten et al. [14] made TEM measurements of the crystallite thicknesses of rod stock GUR415 by shadowcasting, of 30 nm. They also observed microfibrils, of length 0.1 μm, in AFM images of cryogenically fractured surfaces of the moulded material.

Nitric acid degradation followed by gel permeation chromatography (GPC) was first used in 1966 to study polymer single crystals [15] and was soon followed by studies using bulk polymers to investigate structure and reaction mechanisms [16]. The introduction of fuming nitric acid preferentially removes the amorphous regions within the polymer, as the acid molecules diffuse through the structure, attacking and breaking chains on the fold surfaces. Crystalline material is more resistant to attack on the basal plane by the acid due to steric hindrance and hydrogen bonding of the oxidation products [17], although attack on the basal planes can occur, reducing the apparent molecular weight of the crystal chains. The crystal chains that are left, are predominately terminated by carboxyl groups, with about one in eight chains having an NO_2 group at the reactive α position of the dicarboxylic acid chain [18]. The initial attack on the amorphous phase is quite rapid, and the associated drop in molecular weight, and the narrowing of the molecular weight distribution is consistent with random chain scission. Following the removal of the amorphous material, there is a sustained rate of weight loss, as chains are removed from the lateral edges of the crystals [19].

In this paper we shall discuss the use of these nitric acid degradation techniques followed by GPC alongside NMR and DSC measurements to determine the morphology of powder and ram-extruded GUR415 UHMWPE. In particular the nitric acid technique has been applied to examine the difference in thickness of the crystalline lamellae in the two materials.

2. Experimental

2.1. Materials

The UHMWPE samples (nascent powder and moulded rodstock) were obtained from Hoechst-Celanese. The PE is GUR415 grade, molecular weight approximately 6×10^6 g mol^{-1}.

2.2. Nitric acid degradation and GPC

Samples of the powder and moulded forms of the UHMWPE were subjected to degradation by fuming nitric acid for the following times: 12 h; 1 day; 2 days and 4 days. The powder was added to the acid in its raw state, where the particle dimensions were about 200 μm across (it was not possible to break down the structure of the individual particles any further), whilst the well-moulded material was microtomed to a thickness of 8 μm, before treatment. The sealed pots, in which the degradation took place, were put in an oil bath and held at a temperature of 60°C and 100 mg of sample was degraded in 15 ml excess of acid. After the etching time was completed, the pots were opened and the acid diluted in a large excess of distilled water: at least 2 dm^3 per 15 ml of acid. The residue was filtered out and washed with water several times and then with acetone at least twice. The acetone was then dried off overnight in a vacuum oven at room temperature. The etched samples were characterised by GPC, in a solvent of 1,2,4 trichlorobenzene at BP-Amoco, Grangemouth, on a Waters 150CV, using standard methods.

It was necessary to check that any reduction in the degradation reaction rate was due to the presence of stable polyethylene crystals, after the removal of the amorphous component, as opposed to a reduction in the strength of the acid during the experiment. Therefore, the acid was standardised against sodium carbonate before and after etching, making sure it was one of the longest etching times which was chosen, to determine any change in concentration over the reaction time. Anhydrous sodium carbonate was dried to ensure there was no water present, and a known quantity dissolved in distilled water. The acid was dissolved to one part in 40 to reduce its strength and titrated against the alkali solution with a methyl orange indicator. It was found that before the reaction, the concentration of the acid was 22 ± 2 mol dm^{-3}, and afterwards 23 ± 1 mol dm^{-3}. Thus there was no change in acid strength over the maximum etching time and any change in reaction rate was indeed due to the resistance of the crystallites to degradation once the amorphous component had been removed.

2.3. NMR experiments

All of the NMR measurements have been made on a Chemagnetics CMX-200 spectrometer, operating at

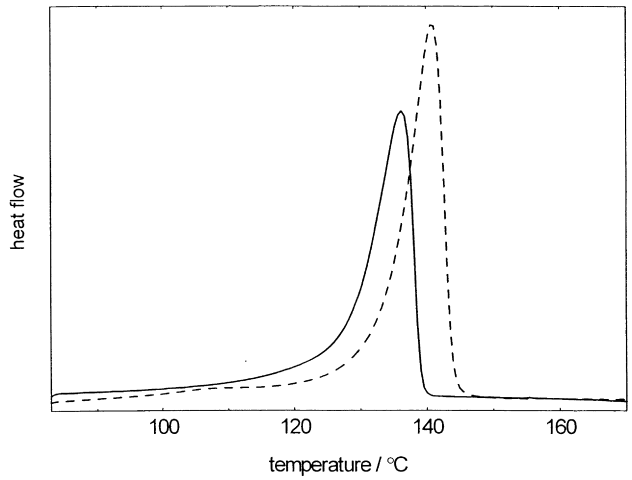

Fig. 1. A comparison of the DSC melting endotherms of the powder (broken line) and the moulded GUR415 (solid line) material.

approximately 200 MHz for protons, and 50.3 MHz for carbons.

The wideline ^{1}H NMR spectra were obtained using a probe with a 5 mm coil, and a 90° pulse width of 2 μs. A standard solid-echo pulse sequence [20] was used (90_x–τ_2–90_y–τ_3–acquire), with the interpulse spacing τ_2 varying between 8 and 31 μs. Here, τ_3 was consistently set at 3 μs less than τ_2 in order to observe the top of the echo. The spectra were fitted to a combination of a modified Gaussian (after Unterforstunghuber and Bergman [21]), to represent the crystalline component, a Lorentzian (amorphous), and an offset term, i.e.

$$y = a\exp\left(-\frac{\nu}{b}\right)^g + \frac{c}{1+d\nu^2} + h \quad (1)$$

A crystalline template was defined to reduce the dependency on fitting parameters by fixing the b and g. All other parameters were allowed to vary. The template was defined by taking a spectrum for each material with a long time spinlock period, such that virtually all the magnetisation in the amorphous phase had been removed, leading to a spectrum with little (some is present by spin diffusion) or no amorphous part, which can be fitted well to the modified Gaussian expression, without the complication of an additional Lorentzian signal. Average values of b and g were 39.1 ± 0.6 kHz and 3.53 ± 0.05, respectively. The offset term, h, was included for completeness, but in practice was very small. Typically h was less than 1% of the spectrum height.

The true FID is only reproduced in the time limit when τ_2 goes to zero (that is to say when $T_2 \gg \tau_2$). The longer the pre-refocus delay is, the bigger the deviation from the true shape. Thus true crystallinity cannot be calculated from a single solid echo spectrum, and a correction is needed to get back to the zero time condition. The correction can be implemented by deconvoluting the spectra according to Eq. (1) for a number of τ_2 values, and extrapolating back to $\tau_2 = 0$. The decay of each of the two components of the spectrum in the echo can be modelled as a Gaussian function [22]:

$$Y = M_0\left(-\left(\frac{\tau_2}{t^*}\right)\right)^2 + c \quad (2)$$

where t^* represents the characteristic time associated with the reduction in the ability of the solid echo to refocus the magnetisation at longer delay times, which is associated with correlations with secondary spin pairs and the dipolar fields of third and fourth order protons. M_0 is the equilibrium magnetisation, and c is an offset term. This was done for the decays of both the crystal and amorphous components. The crystallinity is then the M_0 term in the decay of the crystal component, normalised to the sum of the intercepts of that component and the amorphous phase component. Again the offset term c was included as an aid to the fitting, but was very small. The ratio of c to M_0 was typically less than 4%.

The T_1 relaxation times were measured by the standard inversion recovery experiment with solid echo detection (180_x–τ_1–90_x–τ_2–90_y–τ_3–acquire). The evolution time τ_1 was arrayed between 1 ms and 10 s. The pre refocus delay time (τ_2) was set at 8 μs and the post refocus delay (τ_3) was 5 μs throughout the experiment.

Carbon-13 spectra, recorded under conditions of cross-polarisation, magic-angle spinning and high-power proton dipolar decoupling (CP/MAS/DD) were obtained using the standard pulse sequence. The spinning speed was about 3.5 kHz, with a contact time of 1 ms. The pulse width for the proton excitation was 4 μs, the Hartmann–Hahn match was 62.5 kHz, and the decoupling field strength was 82 kHz.

2.4. DSC experiments

The DSC was carried out on a Perkin–Elmer DSC7 at a heating rate of 10°C min^{-1}, calibrated against indium and zinc. The crystallinity was calculated by dividing the area under the melting endotherm by the heat of fusion for a 100% crystalline sample, taken [23] as 293 J g^{-1}.

3. Results and discussion

The DSC experiments (the melting curves for which are shown in Fig. 1), show that the powder has a higher melting point at 414 K than the moulded material, 409 K. Hoffman et al. [24] showed that the melting point of a semi crystalline material, T_m, can be related to the average thickness of the crystallites within it. The relation is of the form:

$$d_x = \frac{2\sigma_e}{\Delta h_f}\left(1 - \frac{T_m}{T_m^\circ}\right)^{-1} \quad (3)$$

where d_x is the crystal size; T_m° is the melting temperature of a crystal of infinite thickness, 418.95 K; σ_e is the surface free energy, 9.3×10^{-2} J m^{-2} and Δh_f is the heat of formation of the crystal, 2.80×10^8 J m^{-2} [24].

Using Eq. (3), these melting points correspond to average

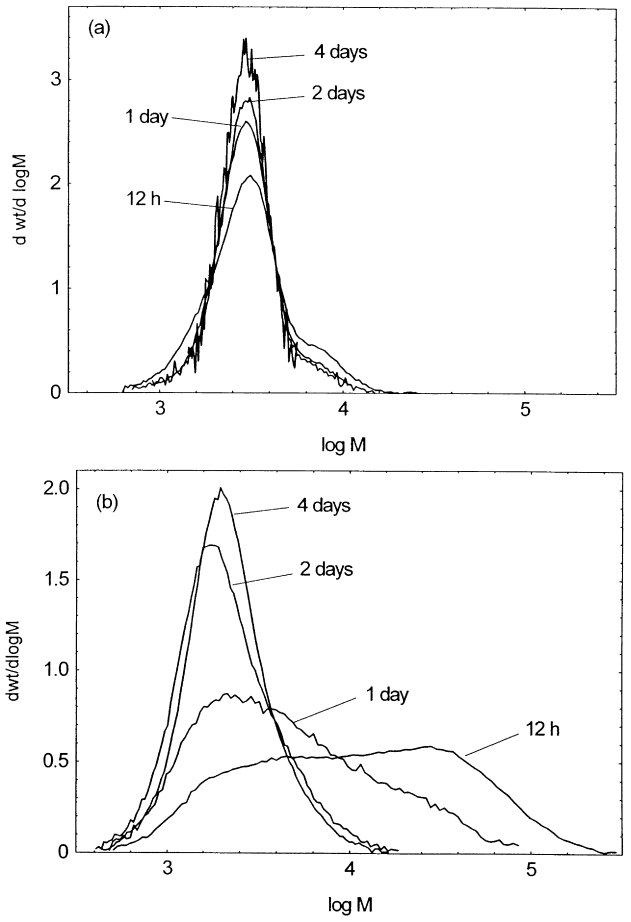

Fig. 2. GPC chromatograms of the etched moulded material (a) and the etched powders (b). The etching times are indicated.

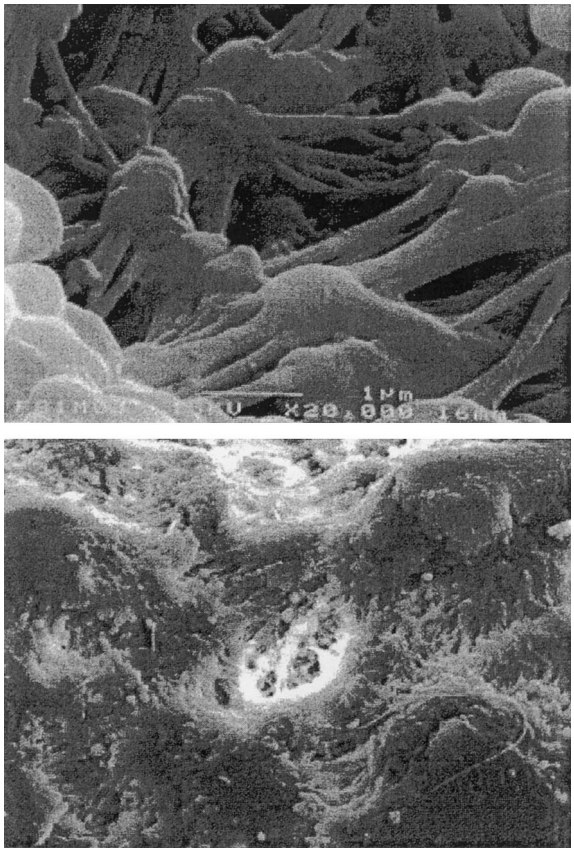

Fig. 3. SEM micrographs of a powder particle, taken from those etched for 12 h in fuming nitric acid. The scale bar in the top image is 1 μm, the lower image being somewhat lower magnification. Fibrillar structures are clearly revealed as the etching has opened up the powder structure revealing some of the internal features. The longer thread-like structures in the lower image are fibres carried through from the filter paper in the cleaning and washing of the polyethylene immediately after etching.

crystal thicknesses of 58 ± 13 nm for the powder and 28 ± 4 nm for the moulded material. They are also associated with crystallinities of $62 \pm 2\%$ and $52 \pm 2\%$, respectively. It is suggested however, that the melting temperature is artificially increased due to the peculiar morphology associated with the reactor powder and is therefore not a fair reflection of the crystallite size. Thus it is desirable to use a different method with which to determine the crystal thickness directly. One way to do this is by nitric acid degradation, followed by GPC.

The GPC chromatograms for the etched powder and moulded material samples are shown in Fig. 2. Usually, the best etching time, where most of the amorphous material has been removed, and any further reduction in mass comes from material which is being stripped off the lateral crystal surfaces, is found by looking for a change in the slope of the associated weight loss curve. Alternatively, if the peak molecular weight does not change, that means that the length of the chains in the crystals is not being reduced any further. Thus at any time after this, the crystal chains are not being reduced in length by attack on the basal planes. The peak molecular weight cannot generally however, be assumed to be the best value for the average molecular weight of the system. The peak position goes as $(\overline{M_w M_n})^{1/2}$, and so is only a reasonable value for the average molecular weight when the polydispersity index is low [19]. In this work it is seen that in the moulded GUR415 there is no change in the slope in the weight loss curve, but there is also no accompanying shift in the position of the peak in the GPC molecular weight distribution. To get a value for the average crystal stem length, the curve of average molecular weight against etching time has been fitted to a decreasing exponential, which is a purely phenomenological expression, and the resulting long-time offset taken as the equilibrium stem length. The same method was also applied to the powder samples. In Fig. 2, it can be seen that, for the powder, there is an initial bimodal distribution in the molecular weights, with the higher molecular weight peak at 32,000 g mol^{-1}, which corresponds to a stem length of 283 nm. This is much higher than the stem length determined from the final position of the peak in the powder distribution in the 4 day etched material (1584 g mol^{-1} leading to 14 nm) and is probably due to extended chain crystals which are removed completely by lateral attack at the longer

Table 1
The weight (M_w) and number (M_n) average molecular weights of the etched powder and moulded material, calculated from the GPC distributions shown in Fig. 2, together with the crystalline stem lengths with and without the 35° chain tilt correction

	M_w (±5%) (g mol^{-1})	M_n (±10%) (g mol^{-1})	Stem length from M_w (nm)[a]	Stem length from M_w (nm)[b]
Powder:12 h	22770	4700	206 ± 10	170 ± 8
1 day	8317	2699	75 ± 4	62 ± 3
2 days	2556	1742	23 ± 1	18.8 ± 0.9
4 days	2478	1851	22 ± 1	18.3 ± 0.9
Moulded 12 h	3482	2591	32 ± 2	26 ± 1
1 day	3249	2689	29 ± 1	24 ± 1
2 days	3190	2726	28 ± 1	23 ± 1
4 days	2976	2752	27 ± 1	22 ± 1

[a] Without chain tilt correction.
[b] With 35° chain tilt correction.

etching times. It is unlikely that this higher molecular weight peak is due to unreacted polymer with the acid not fully penetrating the powder particles, since the molecular weight is nowhere near as high as the expected molecular weight of the full polymer chain at 6×10^6 g mol^{-1}. Scanning electron microscopy (SEM) (Fig. 3) of the 12 h etched sample shows regions of fibrillar structures of approximately 1 μm in length which are not present at the longer etching times, and we tentatively suggest that the extended chain morphology is present in these fibrils.

The GPC chromatograms of the etched moulded material are much more dominated by a single peak at about 3000 g mol^{-1}, although there is slight shoulder at 7080 g mol^{-1} in the shortest etch distribution. This shoulder is at a molecular weight, which would correspond to an all *trans* lamellar thickness of about 64 nm, about twice that calculated from the whole distribution (32 nm—Table 1). This shoulder is likely to be due to tie chains extending across a single layer of the amorphous lamellae. A similar peak may exist in the powder distribution for 12 h also, but with the much higher molecular weight material being present any trace of it is totally obscured by the high proportion of much higher molecular weight material.

The position of the main peak in the moulded samples does not change with etching time, whereas the weight average molecular weight of the distribution does decrease, while the peak becomes somewhat sharper. This suggests that in this case the crystal stems are not being reduced in length and that the molecular weight of the chains at long times will be a good approximation to the length of a crystal chain in one lamella. The position of the lower molecular weight peak in the powder's distribution, is however, not fixed: it is still shifting slightly to lower molecular weights even after 4 days. The weight loss curve also shows no change in slope. However, since the weight average molecular weight of the distribution *is* levelling off (as is shown in Fig. 4), the same procedure as was used for the moulded material was applied. Thus the long time molecular weight was used to determine the average lamellar thickness and was estimated by fitting phenomenologically a decreasing

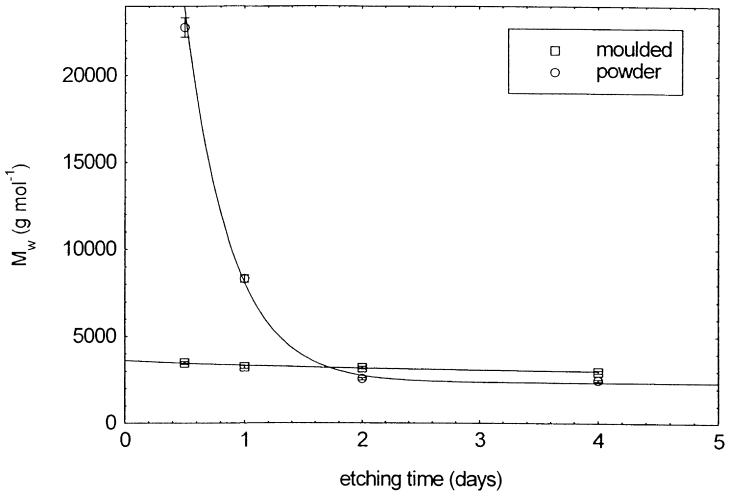

Fig. 4. The decrease in the weight average molecular weights of the powder and moulded GUR415 materials as a function of etching time. The values have been calculated from the GPC distributions shown in Fig. 2. The curves through the data are fits to Eq. (4).

Table 2
Results from fitting exponential decreases to the GPC lamellar thicknesses of the powder and moulded GUR415 materials (Eq. (4)). The last column is taken as the average crystal thickness in the bulk sample, since good agreement is seen between L_w and the longitudinal crystal thickness [18]

Sample	a (g mol^{-1})	τ (nm/day)	M_w (GPC) (g mol^{-1})	L_w (GPC) (nm)[a]	L_w (GPC) (nm)[b]
Powder	80000 ± 20000	0.38 ± 0.05	2340 ± 220	21 ± 1	17 ± 1
Moulded	710 ± 180	2 ± 2	2913 ± 234	26 ± 1	21 ± 1

[a] Without chain tilt correction.
[b] With 35° chain tilt correction.

exponential to the data; the offset corresponding to this quantity, as is shown below.

$$y = a \exp(-t/\tau) + M_{w(GPC)} \quad (4)$$

The data were fitted using the Easyplot 4.0.1 software, applying the Levenberg–Marquardt fitting algorithm. Good agreement has been seen between the weight average derived crystal thickness [19] and the longitudinal crystal thickness determined by X-ray techniques [25] in linear high density polyethylene. Thus the crystal thickness derived from the weight averages of the molecular weight distributions in Fig. 2 have been plotted in Fig. 4.

It is still desirable to allow for chain tilt in deriving a final value for the crystallite thickness: in general the chains in the all-trans conformation do not lie perpendicular to the plane of the crystal surface, containing the chain folds. Different angles for chain tilt have been reported. Keller and Sawada [26] report an angle of 35° for slow cooled polyethylene and 17.5° for quenched. For polyethylene in general, Bartczak et al. [27] report an angle of 27°. The correction is made by multiplying the stem lengths by cos θ, where θ is the angle of tilt. The values quoted in Table 1 are both those corrected for chain tilt (assuming the maximum tilt angle of 35°) and the uncorrected versions. The actual molecular weights are plotted against etching time in Fig. 4 and these have been subsequently converted to lamellar dimensions.

The results from fitting the molecular weight data to Eq. (4) show that the average crystal lamellar thicknesses in the moulded material and in the powder are of the same order at 21 ± 1 and 17 ± 1 nm, respectively. The parameters from the fit are shown in Table 2. Since these measurements are a physical measure of the length of the chains, which are in the crystallites, then it is clear that, as discussed previously, the DSC gives a misleading prediction of their thicknesses.

Table 3
Crystallinity (as measured by NMR) and average proton T_1 relaxation times of the etched powders, with etching time

Powder etch time (days)	Average ^{1}H T_1 (ms)	NMR crystallinity (%)
0	713 ± 24	60 ± 1
0.5	1113 ± 16	73 ± 1
1	1483 ± 23	92 ± 2
2	1976 ± 31	96 ± 2
4	2290 ± 40	98 ± 3

In fact, while Hoffman's values work fairly well, the values of the crystal thickness from the DSC are very model dependent. It should be noted that different authors [28–30] give different values for the "constants" in Eq. (3): the infinite crystal melting temperature; the surface free energy and the heat of formation of the crystal. We have used Hoffman's data here, because the use of some other authors' data produce unphysical (too large or even negative) values for the lamellar thickness. The fact that the average thickness of the lamellae in the powder is slightly smaller than that in the moulded material may be a reflection of the continued shift

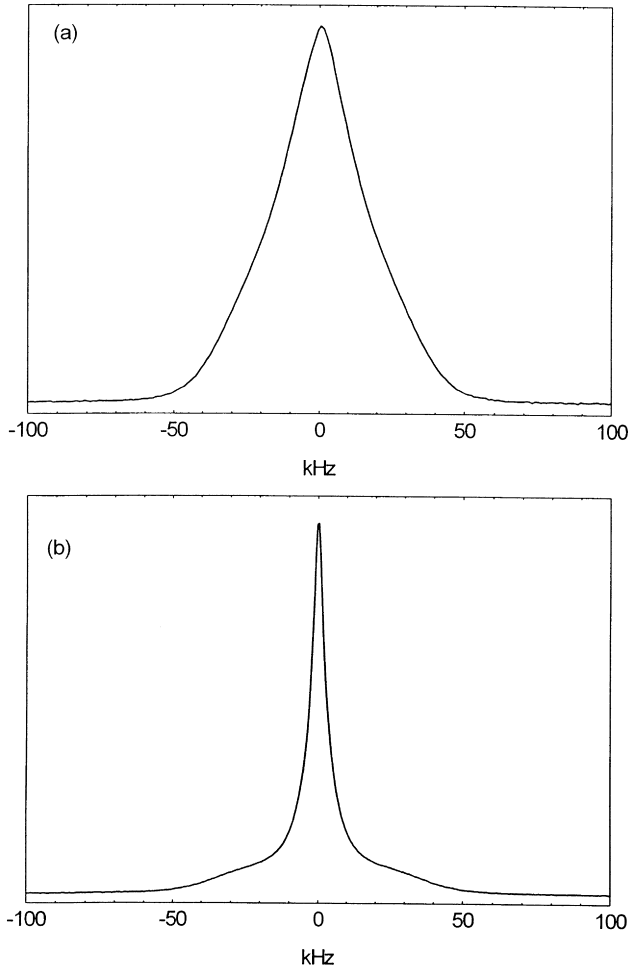

Fig. 5. The wide-line proton NMR spectra of the powder (a) and moulded (b) GUR415 materials.

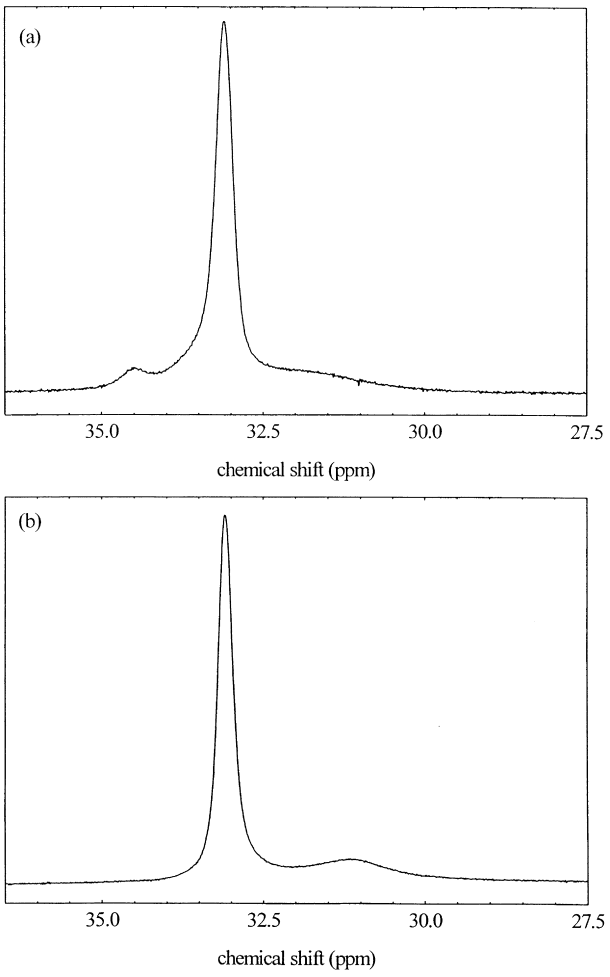

Fig. 6. CP-MAS high resolution ^{13}C NMR spectra of the powder (a) and moulded (b) GUR415 materials.

in the position of the peak in the molecular weight distribution: there is a slight attack on the surfaces of the crystallites. Alternatively it could be explained by a small amount of annealing during processing. The higher crystallinity, while not being a manifestation of a small number of large crystals can be attributed to the extra crystal structures associated with the fibrils that are removed on significant etching.

The crystallinities of the etched powders have been measured by the NMR method discussed in Section 2. These are shown in Table 3, and despite the small component in the spectrum characteristic of mobile material are shown to have a very high crystallinity when etched. There would not be much to gain by further etching. This lends extra credence to the assumption that it is possible to use these stem length values in the same way as has been done for the moulded material, given that there is not much degradation into the crystals themselves up to this time.

It is interesting to note that when there is no chain tilt considered, the thickness of the moulded material's crystallites from the nitric acid/GPC method matches well the thickness derived by DSC. However for the reasons discussed above, the DSC does not necessarily give an accurate projection of the crystal thickness in either the powder or the moulded material.

Observations of proton NMR spectra of the nascent powder and the moulded GUR415 (Fig. 5) show that there are clear distinctions between the two materials. Usually, the spectrum of polyethylene at room temperature shows two distinct components, a broad, Gaussian-type part, and a narrower, Lorentzian part, assigned to the crystalline and amorphous phases, respectively. This is essentially due to the extent to which molecular motion can average the proton dipolar interactions. At room temperature, the amorphous component is well above its glass transition temperature, and therefore undergoes rapid motion, which effectively averages out the dipolar interactions on the time scale of the NMR experiment, producing a relatively narrow Lorentzian. On the other hand, the crystalline phase is relatively rigid, and the dipolar interactions in this component are not averaged, which produces the broad component in the spectrum. The spectrum of the powder (Fig. 5a) shows much less distinction between the two components than that of the moulded material, which is why it was particularly important to define template values for use in Eq. (1) for the powder, because the distinction between crystalline and amorphous components is poor. The broad character of the Lorentzian part of the spectrum implies that the mobility of at least part of the amorphous phase in the powder is somewhat more restricted than in the moulded material, where the amorphous component is represented by a much narrower peak. The NMR crystallinities, determined using the method described in the Experimental part, have been calculated as $60 \pm 1\%$ for the powder, and $55 \pm 1\%$ for the moulded material, agreeing fairly well with the DSC measurements.

The ^{13}C CP-MAS experiments are shown in Fig. 6. The spectrum of the moulded material (6b) shows two clear peaks, which have been well established as arising from the crystalline phase (33 ppm) and the amorphous phase (a broader peak around 32 ppm). Consistent with the observations made by Morin et al. [11], Fig. 6(a) shows that the powder's amorphous phase has fewer bonds in the gauche conformation than in the moulded material, or a slower rate of exploration of states in that phase. The evidence for this lies in the positions of the peaks corresponding to material in the amorphous phase. The peak due to amorphous material in the powder is not shifted as far upfield as the corresponding peak in the moulded material's spectrum, as can be seen in Fig. 6. A further feature of the CP-MAS spectrum of the powder is the presence of a distinct peak at 34.5 ppm, downfield from the orthorhombic crystal peak, which is associated with the presence of monoclinic crystal material, which is itself associated with polymer crystals under stress [31], consistent with the idea of the "strained" morphology suggested by Morin et al. [11], producing frozen-in stress. This monoclinic crystal material is removed on processing, but can be recovered by subjecting the moulded material to

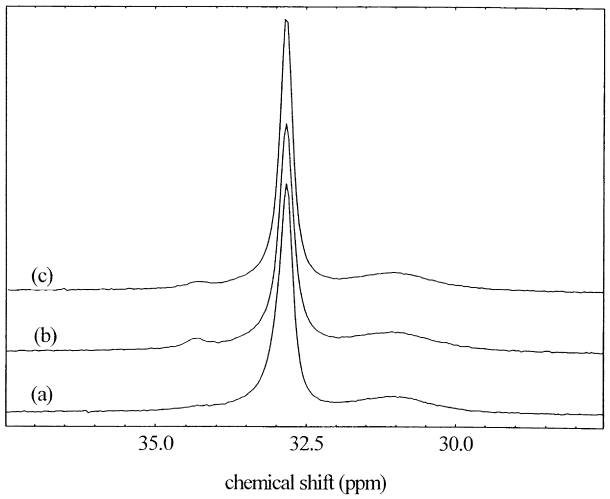

Fig. 7. High resolution ^{13}C CP-MAS NMR spectra of samples of the moulded GUR415 material. (a) Original sample, (b) after creep in compression (16 MPa 23 days) and (c) after three months recovery.

fairly low levels of compressional stress (16 MPa for 22.8 days—Fig. 7). All this evidence indicates a morphology in the powder which has significant differences to the morphology in the moulded material.

It is known that while the T_1 relaxation time measured by the inversion recovery method is a weight average of the relaxation rates in the components of the system [32], it is difficult to get an accurate measure of the relaxation time in the distinct phases of solid polyethylene due to the intrinsic averaging associated with spin diffusion. Therefore these samples of UHMWPE powder, etched with nitric acid, should provide an excellent system from which to get a good estimate of the crystal T_1, since most of the amorphous phase material is removed after only several days degradation. The spin–lattice relaxation curves for each sample are shown in Fig. 8 and the T_1s for the subsequent etches have been plotted against etching time and then fitted to a rising exponential as shown in Fig. 9. This leads to a relaxation time which would be for a 100% etched material, and thus a 100% crystalline polyethylene. This relaxation time is 2500 ± 100 ms. This is a lot longer than the value measured through the decay of the all-trans peak in a T_1 experiment with detection via cross polarisation [33] (900 ± 65 ms), which is still effected by spin diffusion during the measurement. In the etched powder samples there is less and less amorphous phase with which the crystal phase can exchange spin polarisation, so there is much less averaging of the intrinsic relaxation times, up to 4 days where the T_1 measured is almost equivalent to that of the extrapolated value.

4. Conclusions

Despite the suggestions to the contrary by DSC experiments, the lamellar thicknesses of the crystallites in powder UHMWPE have been shown to be of the same order as those in the moulded material, in fact a little smaller. This may be due to the crystals being eaten into by the acid during the degradation or alternatively may result in a small amount of annealing during processing. The powder is seen to have a different initial morphology to the moulded material, in that there is the bimodal distribution in the GPC-measured molecular weight distribution for the 1 day etched sample. This, coupled with SEM observations of fibrillar structures in that sample, suggests that there are extended chain crystals present, probably in the fibrils, which lead to higher crystallinity in the powder. The other major differences between the powder morphology and the morphology in the moulded material are the more restricted amorphous phase and the presence of monoclinic crystals in the former. Both these observations agree with the assertion of a morphology possessing considerable strain.

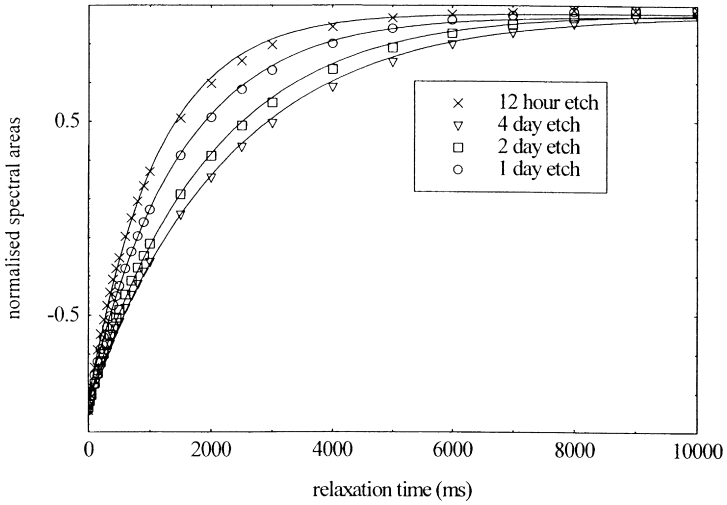

Fig. 8. Spin–lattice relaxation recovery curves for the etched powder samples. As the etching time increases and more of the amorphous material is removed, the T_1 recovery time increases.

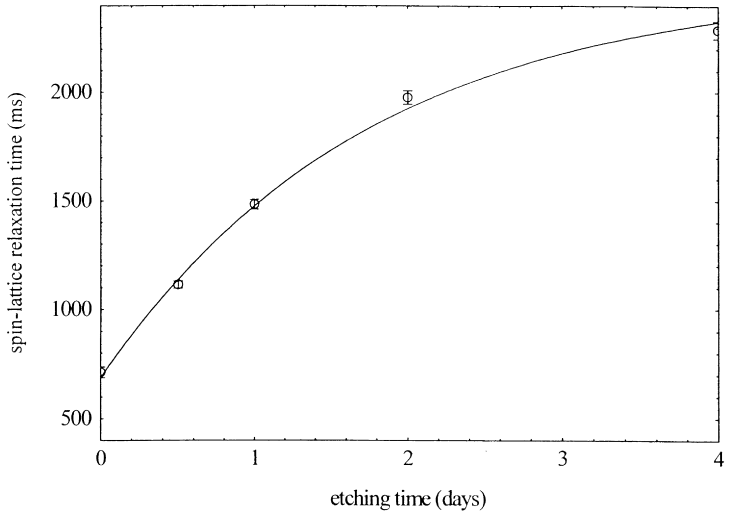

Fig. 9. Graph showing the increase of the spin–lattice relaxation time as a function of etching time. The data have been fitted to an exponential increase, leading to a estimate of the ^{1}H T_1 in 100% crystalline polyethylene of 2500 ± 100 ms.

Measurements of the spin–lattice relaxation times in the etched powders lead to an estimate of the T_1 in 100% crystalline polyethylene of 2500 ± 100 ms. The fact that the crystallinity in the 4 day etched powder is close to 100% shows that confidence can be assigned to the choice of analysis in determining the long time crystal thickness, and hence the thickness of the crystal lamellae.

Acknowledgements

We wish to thank Dr L. Rose (BP-Amoco, Grangemouth) for carrying out the GPC analysis.

References

[1] Li S, Burstein AH. J Bone Jt Surg A 1994;76(7):1080.
[2] Wrona M, Mayor MB, Collier JP, Jensen RE. Clin Orthop Relat Res 1994;299:92.
[3] Rose RM, Crugnola AM, Ries MD, Cimino WR, Paul IL, Radin EL. Clin Orthop 1979;145:277.
[4] Rose RM, Radin EL. Biomaterials 1990;11:63.
[5] DelPrever EB, Crova M, Costa L, Dallera A, Camino G, Gallinaro P. Biomaterials 1996;17:873.
[6] Grood ES, Shastri R, Hopson CN. J Biomed Mater Res 1982;16:399.
[7] Bostrom MP, Bennett AP, Rimnac CM, Wright TM. Clin Orthop Relat Res 1994;309:20.
[8] Premnath V, Harris WH, Jasty M, Merrill EW. Biomaterials 1996;17:1741.
[9] Farrar DF, Brain AA. Biomaterials 1997;18:1677.
[10] Zachariades AE, Kanamoto T. Polym Engng Sci 1986;26:658.
[11] Morin FG, Delmas G, Gilson DFR. Macromolecules 1995;28:3248.
[12] Chanzy HD, Bonjour E, Marchessault RH. Coll Polym Sci 1974;252:8.
[13] Tervoort-Engelen YMT, Lemstra PJ. Polym Comm 1991;32:343.
[14] Valotten P-H, Denn MM, Wood BA, Salmeron MB. J Biomater Sci: Polym Ed 1994;6:609.
[15] Blundell DJ, Keller A, Ward IM, Grant IJ. J Polym Sci: Polym Lett 1996;4:781.
[16] Ward IM, Williams G. J Polym Sci A-2 1969;7:1585.
[17] Capaccio G, Ward IM, Wilding MA, Longman GW. J Macromol Sci: Phys B 1978;15:381.
[18] Rueda DR, Cagaio E, Baltá-Calleja FJ. Colloid Polym Sci 1983;261:626.
[19] Capaccio G, Ward IM. J Polym Sci: Polym Phys 1982;20:1107.
[20] Powles JG, Strange JH. Proc Phys Soc (London) 1963;82:6.
[21] Unterforstunghuber K, Bergman K. J Magn Res 1979;33:483.
[22] Boden N, Levine YK. Mol Phys 1975;29:1221.
[23] Wunderlich B. Crystal melting, Macromolecular physics, 3. New York: Academic Press, 1980.
[24] Hoffman JD, Davis GT, Lauritzen JI. In: Hannay NB, editor. Treatise on solid state chemistry, 3. New York: Plenum Press, 1978.
[25] Clements J, Jakeways R, Ward IM. Polymer 1978;19:639.
[26] Keller A, Sawada S. Makromol Chem 1964;74:190.
[27] Bartczak Z, Cohen RE, Argon AS. Macromolecules 1992;25:4692.
[28] Stack GM, Mandelkern L, Voigt-Martin IG. Macromolecules 1984;17:321.
[29] Shahin MM, Olley RH, Bassett DC, Maxwell AS, Unwin AP, Ward IM. J Mater Sci 1996;31:5541.
[30] Wlochowicz A, Eder M. Polymer 1984;25:1268.
[31] Bevis MJ, Allen PJ. Surface and defect properties of solids, Specialist periodicals reports, 3. The Chemical Society, 1974 chap. 3.
[32] McBrierty VJ, Douglass DC, Kwei TK. Macromolecules 1978;11:1265.
[33] Cook JTE. PhD thesis, University of Leeds, 1998.